JACS
JOURNAL OF THE AMERICAN CHEMICAL SOCIETY
Article
Cite This: J. Am. Chem. Soc. 2020, 142, 641−648
pubs.acs.org/JACS

Pauli Paramagnetism of Stable Analogues of Pernigraniline Salt Featuring Ladder-Type Constitution

Xiaozhou Ji,[†] Haomiao Xie,[†] Congzhi Zhu,[†] Yang Zou,[‡] Anthony U. Mu,[†] Mohammed Al-Hashimi,[§] Kim R. Dunbar,[†] and Lei Fang*[,†]

[†]Department of Chemistry, Texas A&M University, College Station, Texas 77843-3255, United States
[‡]Shenzhen Key Laboratory of Polymer Science and Technology, College of Materials Science and Engineering, Shenzhen University, Shenzhen 518060, China
[§]Department of Chemistry, Texas A&M University at Qatar, P.O. Box 23874, Doha, Qatar

Supporting Information

ABSTRACT: Polyaniline derivatives represent one of the most widely used classes of conductive polymers. The fundamentally important electronic properties of pernigraniline salts, the fully oxidized and acid-doped derivatives of polyanilines, however, are still not well-understood due to their poor stability and configurational uncertainty. To address these issues and to synthetically access stable analogues of pernigraniline salts, ladder-type constitution was imparted into a series of model oligomer analogues with rigid backbones constituted by up to 27 fused rings. The syntheses were achieved through iterative cross-coupling reactions followed by cyclization and oxidation. In contrast to their unstable non-ladder-type counterparts, these ladder-type pernigraniline-like molecules all adopt a well-defined all-*trans* configuration and demonstrate an excellent chemical stability after protonation, rendering it possible to reveal the intrinsic electronic and magnetic properties of molecules resembling pernigraniline. Protonated salts of these oligomers feature a significant diradicaloid open-shell resonance contribution. A dominant temperature-independent Pauli paramagnetism was observed in the solid state, an indication of the delocalization nature of the polarons in ladder-type analogues of pernigraniline salt.

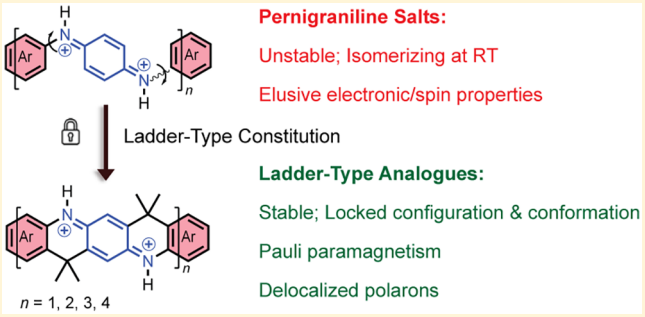

INTRODUCTION

A ladder-type macromolecule consists of an uninterrupted sequence of rings with adjacent rings joined to each other through at least two atoms on one side and two on the other side.[1,2] In contrast to non-ladder-type macromolecules, ladder oligomers and polymers feature high backbone rigidity and lack configurational or conformational disorders.[3,4] Conjugated ladder-type compounds have shown excellent optical and electronic properties suitable for applications in organic light-emitting diodes,[5] organic field-effect transistors,[6,7] and organic photovoltaics,[8−10] as a result of their extended π-delocalization and strong intermolecular coupling facilitated by their rigid coplanar structure.[11] Ladder-type macromolecules also often possess outstanding thermal and chemical stability,[12,13] which enables their potential applications in harsh conditions. The implementation of ladder-type constitution into functional conjugated polymers, such as polyaniline (PANI), is a promising strategy to achieve well-defined configuration/conformation and to improve the stability of these polymers, paving the way for the establishment of their intrinsic structure−property correlations and consequently their potential applications.

PANI derivatives represent one of the most widely used classes of conductive polymers, applied in a great variety of fields, such as anticorrosive coatings,[14] energy storage systems,[15−17] and electrochromic devices,[18,19] among others. In addition, their intriguing multistage redox chemistry, doping processes, and magnetic properties have been the subject of fundamental research for decades.[20−26] Among the PANI derivatives with variable redox states, the partially oxidized derivative, emeraldine base, can be doped by acid to afford a highly conductive emeraldine salt, exhibiting both Curie paramagnetism and Pauli paramagnetism.[27] The fully oxidized, acid-doped counterpart, the pernigraniline salt (Figure 1), was hypothesized to possess dominant bipolaron resonance due to Coulombic repulsion[28,29] and to act as an insulator because of the strong localization of the bipolarons.[30] Recently, *in situ* electrochemical conductivity measurements on stabilized pernigraniline salts, however, indicated[31] that they may be intrinsically conductive. Unfortunately, in-depth and rigorous investigation of pernigraniline salts is severely limited to date.[32−35] First, pernigraniline salts suffer from poor stability as they readily degrade through hydrolysis,[33] reduction,[32,36−38] and conjugated addition[39] at ambient conditions. Efforts have

Received: November 22, 2019
Published: December 12, 2019

DOI: 10.1021/jacs.9b12626
J. Am. Chem. Soc. 2020, 142, 641−648

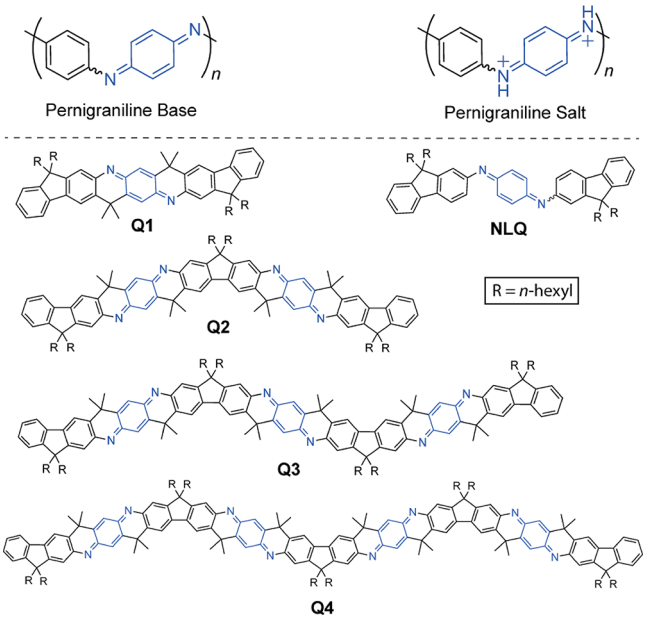

Figure 1. Structural formulas of pernigraniline base, pernigraniline salt, NLQ, and ladder-type oligomeric analogues of pernigraniline base **Q1**–**Q4**.

been made in stabilizing them by chemical modification[30] or protection, which have met with limited success.[31,40,41] Second, the uncontrollable *cis*/*trans* isomerization of the iminium bonds[42] and the torsional rotation of the backbone give rise to structural complexity of pernigraniline salts and discrepant results of their reported properties.[25,30,31,33]

In this context, there is an urgent need to solve the stability and isomerization issues before further fundamental investigations and practical applications of pernigraniline salt derivatives can be conducted rigorously and extensively. Herein, we report a strategy to address these issues simultaneously by implementing a ladder-type constitution in analogues of pernigraniline salts. A series of oligomeric, ladder-type derivatives were synthesized, comprehensively investigated, and compared to a non-ladder-type control compound, the results of which revealed enhanced stability and unexpected Pauli paramagnetism produced by the ladder-type constitution.

RESULTS AND DISCUSSION

In this work, a series of ladder-type pernigraniline oligomers, **Q1**–**Q4** (Figure 1), rather than polymers, were selected as the subjects of investigation to circumvent issues associated with ladder polymers, such as polydispersity, structural defects, and limited solubility.[43−49] In addition, the series of ladder oligomers with well-defined structures and variable sizes allow for the study of precise property evolution from a small molecule to a polymer. **Q1**–**Q4** were designed on the basis of the structure of quinonediimine, wherein **Q*n*** contains *n* quinonediimine units. Bridging dimethylmethene units were installed to fuse the neighboring units into a rigid coplanar ladder-type constitution while fixing the imine bond into a *trans*-configuration. To ensure

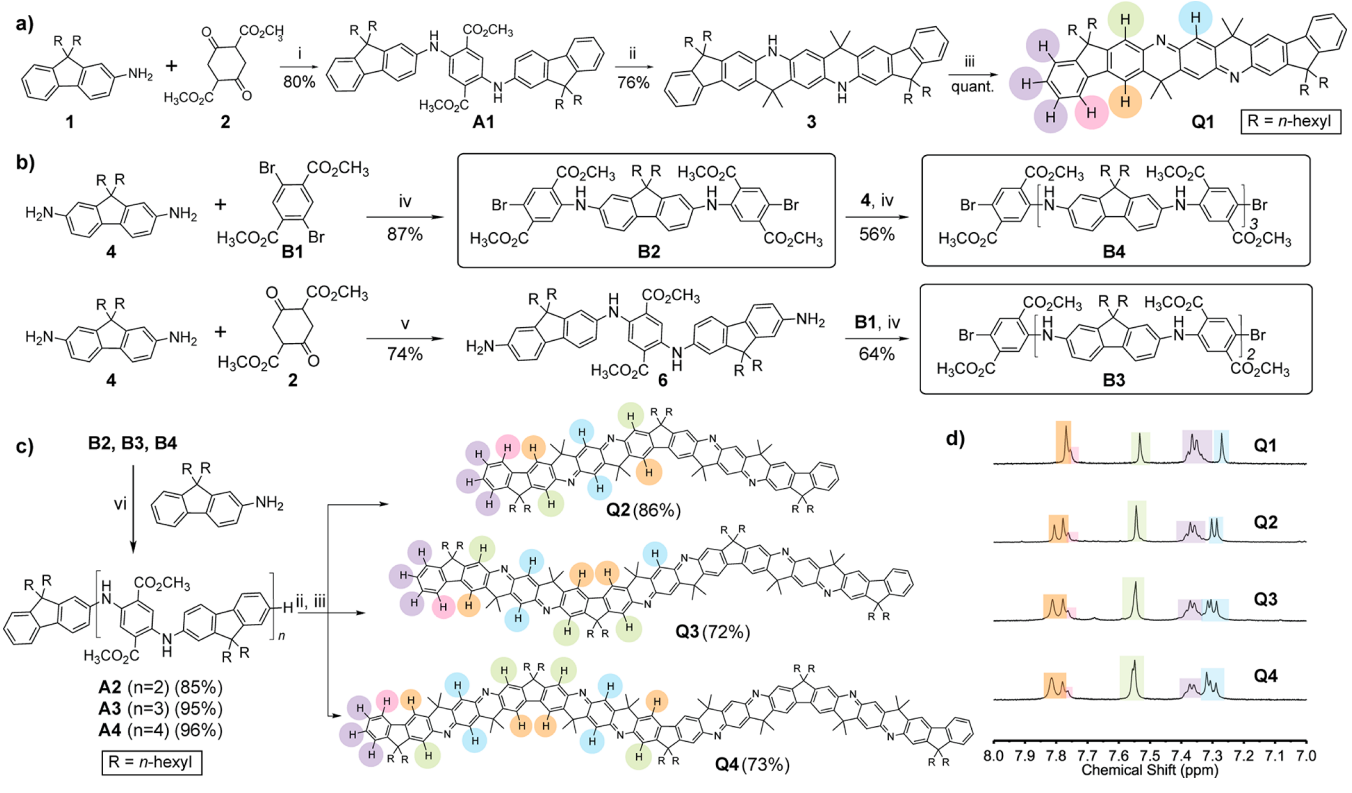

Figure 2. (a) Synthesis of **Q1**. Reaction conditions: (i) molar ratio **1**:**2** = 2.5:1, PTSA (0.2 equiv), ethanol, 80 °C, in air; (ii) CH_3MgBr (10 equiv), THF, 40 °C; then $BF_3{\cdot}Et_2O$, dichloromethane, rt; (iii) Ag_2O, THF, rt. (b) Synthesis of dibromo-functionalized intermediates **B2**, **B3**, and **B4**. Reaction conditions: (iv) $Pd(OAc)_2$ (10 mol %), Xantphos (15 mol %), Cs_2CO_3 (4 equiv), toluene, 110–120 °C; molar ratio $[NH_2]$:[Br] = 1:2; (v) PTSA (0.2 equiv), DMF, 110 °C, in air. (c) Synthesis of **Q2**, **Q3**, and **Q4**. Reaction conditions: (vi) $Pd_2(dba)_3$ (10 mol %), BINAP (30 mol %), Cs_2CO_3 (4 equiv), toluene, 120 °C; molar ratio $[NH_2]$:[Br] = 1.5:1. (d) Downfield regions (7.0–8.0 ppm) of the ^1H NMR spectra of **Q1**, **Q2**, **Q3**, and **Q4** with color-coded labels (500 MHz, $C_2D_2Cl_4$, 298 K).

DOI: 10.1021/jacs.9b12626
J. Am. Chem. Soc. 2020, 142, 641−648

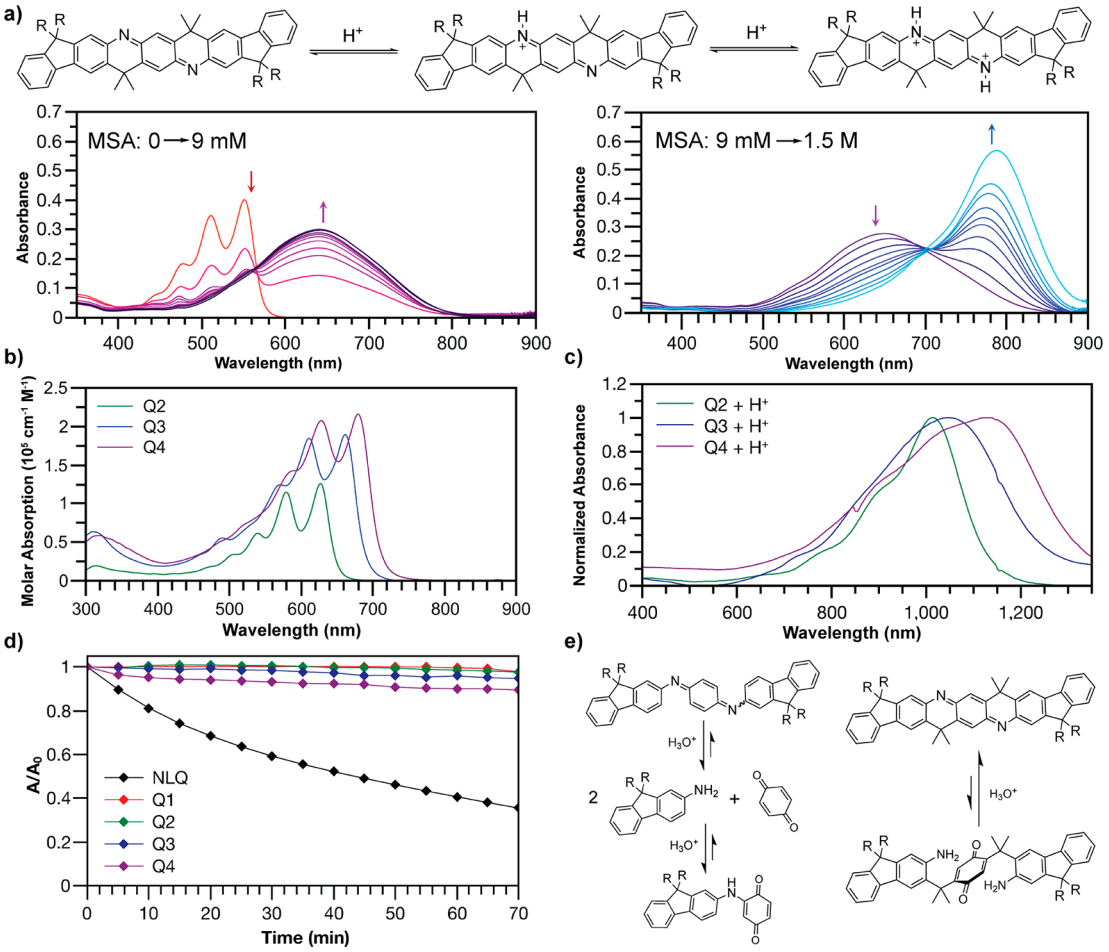

Figure 3. (a) UV−vis absorption spectra corresponding to the two stages of protonation processes of **Q1** in THF with increasing amount of MSA; UV−vis absorption spectra of (b) **Q*n*** (n = 2−4) in toluene and (c) protonated **Q*n*** in trifluoroacetic acid (TFA)/THF (0.44 M) at room temperature. (d) Time-dependent UV−vis absorbance intensity at λ_{max} of **NLQ** and **Q*n*** in MSA/THF solution (0.8 M) at room temperature. (e) Scheme of possible degradation of **NLQ** and **Q1** in acidic conditions.

good solubility, fluorene units with two hexyl groups installed at the 9-position were incorporated into the backbone as the aromatic unit to prohibit overly strong intermolecular $\pi-\pi$ interaction. A control compound **NLQ** was designed as a non-ladder-type analogue, which resembles the constitutional structure of **Q1** except for the lack of the dimethylmethene bridge.

The synthesis of **Q1** started with the preparation of an aniline-like intermediate **A1** through imine condensation between 9,9-dihexyl-2-aminofluorene **1** and dimethylsuccinyl succinate **2**, followed by *in situ* oxidative aromatization under ambient conditions (Figure 2a).[50] The ester groups on **A1**, which are *para* to each other, were used in the subsequent cyclization. Methyl Grignard reagent was first used to convert the ester group into a tertiary alcohol, followed by a regioselective Friedel−Crafts cyclization at the 3-position of the fluorene units promoted by boron trifluoride etherate as a Lewis acid catalyst.[12] The resulting fused-ring product **3** was then further oxidized with Ag_2O to afford the quinoidal molecule **Q1** (Figure 2a), in which the *trans*-configuration is predetermined by the *para* position of the ester groups and locked by the covalent dimethylmethene bridge. This procedure was highly efficient and produced **Q1** on a gram scale. **Q1** exhibited moderate solubility in organic solvents (e.g., 0.4 mg/mL in tetrahydrofuran). The structure of **Q1** was characterized unambiguously by NMR, high-resolution mass spectrometry (HRMS), and single-crystal X-ray diffraction (Figure S19). Synthesis of the control compound **NLQ** was achieved using a similar strategy. Solution-phase ^{1}H and COSY NMR spectra (Figure S1) of **NLQ** revealed the presence of both the *cis* and the *trans* isomers at room temperature in a ratio of 0.42/0.58, in agreement with a previously reported example of pernigraniline base.[42] These configurational isomers dynamically interconvert at room temperature in solution, making it impractical to isolate a pure isomer.

A modified strategy was employed for the synthesis of the longer oligomers **Q2**−**Q4**. First, the linear precursors **B2**, **B3**, and **B4** were synthesized by sequential Buchwald−Hartwig coupling reactions[51,52] of varied combinations of diamino- and dibromo-functionalized intermediates (Figure 2b). In these reactions, the formation of byproducts with higher degrees of oligomerization was suppressed by adjusting the stoichiometric ratio of the starting materials and optimizing the reaction conditions (Table S1), leading to good yields ranging from 56% to 87%. Compounds **B2**, **B3**, and **B4** were then end-capped by **1** through another Buchwald−Hartwig coupling, affording the oligomeric intermediates **A2**, **A3**, and **A4**, respectively, in excellent yields (85−96%) (Figure 2c). Subsequently, ring-annulation and oxidation procedures similar to those for the synthesis of **Q1** were applied to produce the quinoidal oligomer

DOI: 10.1021/jacs.9b12626
J. Am. Chem. Soc. 2020, 142, 641−648

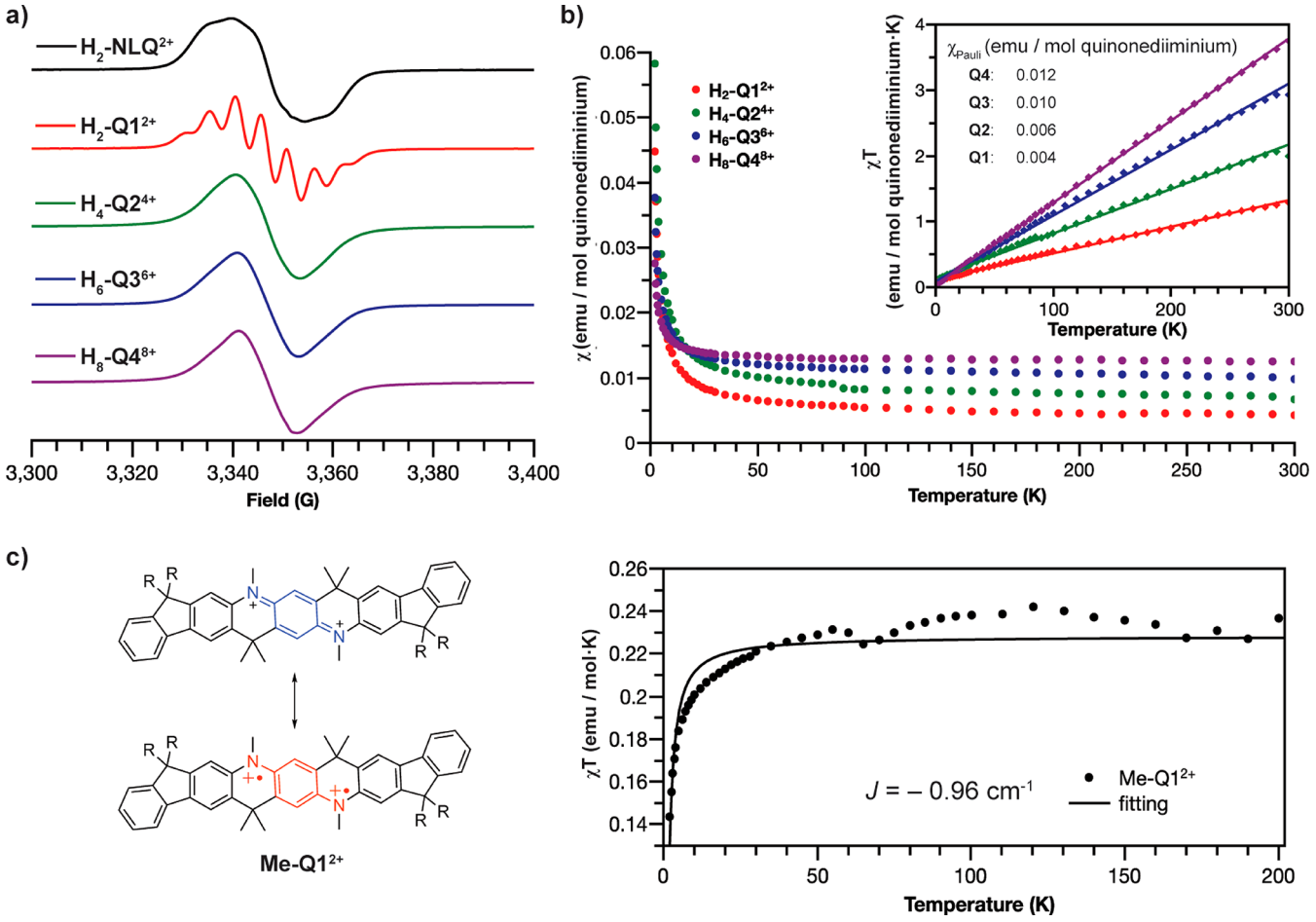

Figure 4. (a) Normalized EPR spectra of protonated **NLQ** and **Q1**−**Q4** in dichloromethane solutions (ca. 10 mM) with TFA (0.1 M) at room temperature. (b) Solid-state magnetic susceptibility (χ) of PTSA-doped **Q*n*** measured over the temperature range of 2−300 K in the powder form; (inset) χT−T plots (dots, experimental data points; lines, linear fitting). (c) Structure of **Me-Q1**$^{2+}$ and χT−T plot of **Me-Q1**$^{2+}$·2SbCl$_6^-$ (dots, experimental data points; line, Bleaney−Bowers fitting).

series **Q2**, **Q3**, and **Q4** in which all of the quinonediimine units are locked into *trans*-configurations. Through this route, the longest oligomer **Q4**, which consists of 27 fused rings, was synthesized in five steps with a 34% overall yield. **Q2**, **Q3**, and **Q4** were isolated as intensely colored powders (ranging from purple to blue) with increased solubility in organic solvents as compared to that of **Q1**. All products were characterized by ^{1}H, ^{13}C NMR, and HRMS. ^{1}H NMR spectra of **Q1**−**Q4** demonstrated that they exclusively adopt the designed *trans*-configuration, in contrast to the undefined and isomerizing configuration of **NLQ**. On the basis of the ^{1}H−^{1}H NOESY NMR spectrum of **Q1** (Figure S21), the resonance signals in the sp^2 region were assigned to the bay region hydrogens (orange and pink), the hydrogens on fluorene unit ortho to the imine bond (green), terminal phenyl hydrogens (purple), and the quinoid hydrogens (blue), from downfield to upfield (Figure 2d). The extension of the molecular size did not impact the patterns and chemical shifts of the NMR signals significantly. The numbers of the sharp signals (blue) of quinoid hydrogens corresponded well with the numbers of distinct repeating units in different chemical environments. In solid-state thin films, despite the rigid backbone, no feature of close π−π interaction was observed in **Q*n*** by grazing incidence wide-angle X-ray scattering (GIWAXS) experiment (Figure S21).

The ladder-type constitution of **Q1**−**Q4** was expected to promote the stability of the corresponding protonated species, leading to unprecedented stable pernigraniline salt derivatives. Upon protonation by Brønsted acids, the absorption bands of these oligomers dramatically red-shifted into the near-infrared (NIR) region, as a result of lowered LUMO levels and smaller bond length alternation of the conjugated core. For example, with the increasing addition of methanesulfonic acid (MSA), **Q1** showed a well-defined two-stage protonation process in THF solution (Figure 3a). The first stage took place with up to 9 mM of MSA, resulting in the monoprotonated **H-Q1**$^+$ with a broad lower-energy absorption band (λ_{max} = 640 nm). In the second stage when the MSA concentration was further increased to 1.5 M, **H-Q1**$^+$ was converted into the fully protonated salt **H$_2$-Q1**$^{2+}$, leading to a strong NIR absorption band (λ_{max} = 798 nm). The well-defined isosbestic points in both stages indicated the clean transformations of **Q1** to **H-Q1**$^+$ and from **H-Q1**$^+$ to **H$_2$-Q1**$^{2+}$ without notable side-reactions. In contrast, the protonation of **NLQ** did not give a clear isosbestic point, likely attributed to the *cis*/*trans* isomerization and decomposition (Figure S5). Similar to **Q1**, oligomers **Q2**−**Q4** also displayed well-defined conversion into the protonated species **H$_{2n}$-Qn**$^{2n+}$ in acidic conditions, with absorption bands further red-shifted to 1020−1190 nm (Figure 3b,c).

DOI: 10.1021/jacs.9b12626
J. Am. Chem. Soc. 2020, 142, 641−648

In drastic contrast with conventional pernigraniline salts and protonated **NLQ**, protonated **Q*n*** were all stable in highly acidic conditions at room temperature. It has been reported that acid-doped pernigraniline salts readily decompose through redox pathway,[32,38] hydrolysis,[35] and conjugated addition.[39] Such degradation was indeed observed on the control compound **NLQ** in our study. In an MSA/THF solution (0.8 M) under ambient conditions, the intensity of the main absorption peak of protonated **NLQ** (840 nm) decreased significantly over the course of 1 h (Figures 3d and S9). Mass spectrometry data of the resulting solution indicated the presence of decomposed products via hydrolysis and further Michael addition[39] (Figure S10). The ladder-type **Q*n*** products exhibited good stability under the same condition with little change in the absorption (Figure 3d) and ^{1}H NMR spectra (Figure S11). The significantly higher chemical stability of the ladder-type molecules can be attributed to the additional strand of bonds, which decreases the entropy gain of the potential hydrolysis of the iminium bonds, rendering the decomposition process less thermodynamically favorable (Figure 3e). It is also noteworthy that, under thermogravimetric analysis (Figure S18), the ladder-type oligomers all showed carbonization yields over 40% as compared to 0% residue weight of **NLQ** at 900 °C, indicating the much higher thermodynamic stability of the sp^2 ladder-type backbones.

The superior stability of the ladder-type pernigraniline salt analogues sets the stage to perform extensive fundamental investigations with ensured structural integrity. In the past, investigation of the magnetic property of conventional pernigraniline salts has been challenging due to the aforementioned poor stability and isomerization issues.[53] In comparison, emeraldine salts have been extensively studied,[27,54] revealing the presence of both Curie and Pauli paramagnetism and providing important insights regarding their remarkable electronic conductivity. Herein, the excellent chemical robustness of protonated **Q*n*** allowed for the examination of the radical characters in pernigraniline salts by electron paramagnetic resonance spectroscopy (EPR).[55] It was hypothesized that, after protonation, the resonance contribution of the open-shell diradical cations increased. Indeed, solution-phase EPR spectra of neutral **Q1**−**Q4** all exhibit weak signals at room temperature with spin densities less than 10^{-3} spins per molecule (Figure S13), a confirmation of their dominant closed-shell resonance. In the presence of TFA (0.1 M), strong EPR signals (g factors = 2.0029−2.0040) with spin densities ranging from 0.3 to 0.8 spins per molecule were observed (Figure 4a), indicating significantly increased open-shell character upon protonation in solution. The well-split EPR signal of **H$_2$-Q1**$^{2+}$ was attributed to the hyperfine coupling of the spins with the nitrogen atoms.[56] In sharp contrast, the non-ladder-type analogue **NLQ** exhibited no well-resolved splitting,[53] likely a result of the configurational isomerization and torsional rotation of the backbone. Broad EPR signals were also observed for the higher oligomers **H$_{2n}$-Q*n***$^{2n+}$ (n = 2−4). The lack of resolved splitting in these cases is attributed to overlapping signals of multiple radical pairs and the complex hyperfine spin coupling with multiple nitrogen atoms in these larger molecules. The open-shell character of protonated **Q1** and **NLQ** was also studied using density functional theory (DFT) calculation, showing a slightly lower diradical character in **H$_2$-Q1**$^{2+}$ (0.65) than that in *trans*-**H$_2$-NLQ**$^{2+}$ (0.70) because the locked coplanar conformation of **H$_2$-Q1**$^{2+}$ favors the closed-shell resonance contribution (Figure S12).

To further understand the magnetic and electronic properties of protonated **Q*n*** in the condensed phase, their spin characters were also investigated in the solid state. Complete protonation of **Q1** was achieved in the solid phase by mixing with 5 equiv of *p*-toluenesulfonic acid (PTSA), which was confirmed by the fact that a thin-film absorption spectrum is similar to that of **H$_2$-Q1**$^{2+}$ in acidic solution (Figure S6). Using this same approach, solid-state **H$_{2n}$-Q*n***$^{2n+}$ samples were prepared by treatment with 5*n* equiv of PTSA. To confirm the structural integrity of these solids after exposure to ambient conditions, they were redissolved and subjected to solution-phase absorption spectroscopy, the results of which were identical to the measurements made before the solid-state acid treatment (Figure S7). EPR spectra of these protonated solids all exhibit broad and strong one-line signals.

In addition to EPR spectroscopy, superconducting quantum interference device (SQUID) magnetic measurements were performed at 2 K to investigate the spin ground states of these pernigraniline salt analogues (Figure S15). The magnetization data for **H$_2$-Q1**$^{2+}$ are in accord with a singlet ground state (S = 0) with a small negative coupling constant (−0.49 K), suggesting a weak antiferromagnetic coupling between the radical pair.[57] Such coupling is likely facilitated by the rigidity and coplanarity of the conjugated ladder-type backbone. In contrast, rigorous solid-state SQUID measurements on protonated **NLQ** were not possible due to its poor stability.

Surprisingly, all of the protonated ladder-type oligomers exhibit dominant temperature-independent paramagnetism (TIP) (Figure 4b). Magnetic susceptibility data obtained from 2 to 300 K revealed constant values. The product of molar magnetic susceptibility and temperature ($\chi_{total}T$) was plotted against temperature, revealing a linear relationship with R^2 > 0.99 [see eq 1]. This TIP behavior is attributed to Pauli paramagnetism, given that van Vleck TIP is only significant in cases of transition metal paramagnets of heavier elements wherein ground states mix with excited states.[58,59] Among **H$_{2n}$-Q*n***$^{2n+}$, the χ_{Pauli} per mole of quinoediiminium unit increases steadily from 4×10^{-3} emu/mol for **H$_2$-Q1**$^{2+}$ to 1.2×10^{-2} emu/mol for **H$_8$-Q4**$^{8+}$, indicating that the TIP is correlated to the size of the extended backbones. The densities of states at the Fermi level $\rho(E_F)$ were calculated to be in the range from 7×10^{25} to 2.2×10^{26} eV^{-1} mol^{-1}. It is also noteworthy that the $\chi_{total}T$ versus T plot exhibited only a very small contribution from Curie paramagnetism (vertical intercepts on the plot), indicating the dominant delocalized nature of spins in the solid states of protonated **Q*n***.

$$\chi_{total}T = C + \chi_{Pauli}T \quad (1)$$

where C is Curie paramagnetism and T is temperature.

Pauli paramagnetism in organic materials (e.g., doped polyacetylene[60] and polythiophene[61]) is commonly indicative of the presence of a metallic polaron lattice, and can serve as a measurement of the density of states near the Fermi level.[62] Among PANI derivatives, a combination of Pauli and Curie paramagnetism was observed in emeraldine salts as a result of the presence of both delocalized and localized paramagnetic centers.[23,27,28] The magnetic susceptibility of conventional pernigraniline salts, however, has not been well-established due to the stability and isomerization issues. In the present case, such measurements were rendered possible by the ladder-type constitution, which not only enhances the stability but also locks the configuration and conformation of these pernigraniline salt analogues. The dominant Pauli paramagnetism observed for protonated **Q*n*** revealed the delocalized nature of the polarons in

DOI: 10.1021/jacs.9b12626
J. Am. Chem. Soc. 2020, 142, 641−648

the solids, in agreement with the recent discovery of high conductivity of a pernigraniline salt film measured in situ by electrochemical methods.[31] To further corroborate the magnetism data, solid-state conductivity measurements were performed on compressed pellets of neutral and protonated **Q1** and **Q2** using a four-probe method (Figure S16); the conductivity of protonated **NLQ** could not be properly measured due to the rapid decomposition. Although limited by insulating hexyl chains and PTSA, as well as significant grain boundaries and disorder in the polycrystalline state, the protonated solids of **Q1** nevertheless showed electrical conductivity up to 10^{-5} S/cm, in a sharp contrast to the insulating nature of pristine **Q1** and **Q2** (conductivity less than 10^{-10} S/cm). In addition, AC impedance measurement of the protonated **Q1** pellet sample revealed that the conductivity was mainly electronic with no observable ionic contribution (Figure S17).

We attributed the delocalization nature of polarons to the intermolecular interaction[63] through the protonated N−H units, which has also been a key factor contributing to the conductivity of emeraldine salts.[64] To confirm this hypothesis, a control compound **Me-Q1**$^{2+}$ (Figure 4c) was synthesized and fully characterized by NMR, MS, and single-crystal X-ray diffraction (Figure S19). The only difference between **Me-Q1**$^{2+}$ and **H2-Q1**$^{2+}$ was the N−CH_3 unit that inhibits the potential intermolecular interaction between N−H groups. DFT calculation on **Me-Q1**$^{2+}$ revealed delocalized spin density with a smaller diradical character (0.51) as compared to that of **H_2-Q1**$^{2+}$ (0.65) (Figure S12). Interestingly, SQUID magnetometer measurements of **Me-Q1**$^{2+}$ showed typical paramagnetic behavior of a localized diradical system,[65−70] dramatically different from that of **H_2-Q1**$^{2+}$. The decrease of χT value at low temperature indicates the antiferromagnetically coupled nature of the diradical. A fitting with the Bleaney−Bowers equation yield a coupling constant $J = -0.96$ cm^{-1}. The small and negative sign of the coupling constant reveals that **Me-Q1**$^{2+}$ possessed singlet ground state, while its singlet and triplet states were almost degenerated. Conductivity of a mixture of **Me-Q1**$^{2+}$ with 5 equiv of PTSA was measured by the same four-probe method described above, showing no observable conductivity (Figure S16). Comparing the different paramagnetic behavior and bulk conductivity of **Me-Q1**$^{2+}$ and **H_2-Q1**$^{2+}$, we confirmed that intermolecular interaction through N−H units was an important factor to facilitate the polaron delocalization in the solid of PTSA protonated ladder-type compound **H_2-Q1**$^{2+}$. Taken together, the observed Pauli paramagnetism and conductivity of these stable ladder-type analogues of pernigraniline salt are incontrovertible evidence for the delocalized polarons of fully oxidized PANI derivatives, findings that address the long-standing challenge in understanding their intrinsic electronic characters.

CONCLUSION

In this work, a series of ladder-type oligomers resembling the structure of pernigraniline bases/salts have been designed and synthesized. With the additional strand of covalent bonds, the conjugated backbones are predetermined to be in an all-*trans* configuration and are locked into a rigid coplanar conformation, allowing for the establishment of a structure−property correlation of pernigraniline salt-analogues excluding the influence of decomposition, isomerization, and torsional disorder. Protonation of these pernigraniline base-analogues led to a pronounced open-shell resonance contribution with high spin density. As compared to conventional pernigraniline salts and the non-ladder-type control compound, these ladder-type oligomers exhibit much higher stability in acidic conditions, enabling fundamental investigations and practical applications of this unique class of organic materials with reliable structural integrity. Interestingly, in the solid state, these pernigraniline salt-like oligomers exhibit a dominant temperature-independent Pauli paramagnetism indicative of the delocalized status of the polarons. A methylated control compound, in contrast, did not show Pauli paramagnetism, confirming the key role of intermolecular interaction for the solid-state polaron delocalization. This observation agrees with their moderate conductivity properties measured in the solid state. Simply put, the ladder-type constitutional design imparts the desired chemical stability and structural certainty into acid-doped PANI materials in high oxidation states, such that their unexpected metallic magnetic and electronic properties can be revealed.

The data and results obtained in this work offer a number of important principles for the design and development of next-generation functional organic materials. First, the employment of ladder-type constitution is demonstrated to be an efficient strategy to stabilize certain conventionally unstable organic materials, particularly those prone to undergo entropy-driven decomposition. Second, this strategy can also be used to lock the configuration and conformation of complex polymer backbones to afford desired properties and to give a much clearer correlation between structural features and properties. Last, in the context of delocalized polarons found in these pernigraniline salt-derivatives, one can anticipate that the bulk conductivity of similar ladder-type analogues can be enhanced by orders of magnitude once the insulating side-chains are shortened and the conjugated backbones are elongated. This goal can be achieved through a processing strategy involving in situ side-chain cleavage[13,71] and backbone oxidation, from a soluble precursor functionalized with cleavable side-chains in its reduced state. Future development in this vein can lead to a new class of highly conductive, metallic organic species.

ASSOCIATED CONTENT

Supporting Information

The Supporting Information is available free of charge at https://pubs.acs.org/doi/10.1021/jacs.9b12626.

General methods, synthesis, and characterization data (PDF)

Crystallographic data of **Q1** (CIF)

Crystallographic data of **Me-Q1**$^{2+}$·2$SbCl_6$ (CIF)

AUTHOR INFORMATION

Corresponding Author

*fang@chem.tamu.edu

ORCID

Congzhi Zhu: 0000-0002-1302-7187

Mohammed Al-Hashimi: 0000-0001-6015-2178

Lei Fang: 0000-0003-4757-5664

Notes

The authors declare no competing financial interest.

ACKNOWLEDGMENTS

L.F. gratefully acknowledges support for this work by the Robert A. Welch Foundation (A-1898) and the Qatar National Priority Research Program (NPRP10-0111-170152). K.R.D. gratefully acknowledges support for this work by the National Science

DOI: 10.1021/jacs.9b12626
J. Am. Chem. Soc. 2020, 142, 641−648

Foundation (CHE-1808779) and the Robert A. Welch Foundation (A-1449). The SQUID magnetometer was purchased with funds provided by the Texas A&M University Vice President of Research. We also thank Dr. Nattamai Bhuvanesh for single-crystal X-ray diffraction measurements, and the Laboratory for Molecular Simulation and High Performance Computing facilities at TAMU for providing software, support, and computer time.

REFERENCES

(1) IUPAC. *Compendium of Chemical Terminology*, 2nd ed. (the "Gold Book"); compiled by McNaught, A. D.; Wikinson, A.; XML on-line corrected version: http://goldbook.iupac.org.
(2) IUPAC. *Compendium of Polymer Terminology and Nomenclature: IUPAC Recommendations 2008*; Royal Society of Chemistry: Cambridge, UK, 2009.
(3) Lee, J.; Kalin, A. J.; Yuan, T.; Al-Hashimi, M.; Fang, L. Fully conjugated ladder polymers. *Chem. Sci.* **2017**, *8*, 2503−2521.
(4) Schlüter, A. D. Ladder polymers: the new generation. *Adv. Mater.* **1991**, *3*, 282−291.
(5) Wu, Y.; Zhang, J.; Fei, Z.; Bo, Z. Spiro-bridged ladder-type poly (p-phenylene) s: towards structurally perfect light-emitting materials. *J. Am. Chem. Soc.* **2008**, *130*, 7192−7193.
(6) Wang, Y.; Guo, H.; Harbuzaru, A.; Uddin, M. A.; Arrechea-Marcos, I.; Ling, S.; Yu, J.; Tang, Y.; Sun, H.; Lo′pez Navarrete, J. T. (Semi) ladder-Type Bithiophene Imide-Based All-Acceptor Semiconductors: Synthesis, Structure−Property Correlations, and Unipolar n-Type Transistor Performance. *J. Am. Chem. Soc.* **2018**, *140*, 6095−6108.
(7) Zhang, W.; Han, Y.; Zhu, X.; Fei, Z.; Feng, Y.; Treat, N. D.; Faber, H.; Stingelin, N.; McCulloch, I.; Anthopoulos, T. D. A Novel Alkylated Indacenodithieno [3, 2-b] thiophene-Based Polymer for High-Performance Field-Effect Transistors. *Adv. Mater.* **2016**, *28*, 3922−3927.
(8) Cai, Z.; Awais, M. A.; Zhang, N.; Yu, L. Exploration of Syntheses and Functions of Higher Ladder-type π-Conjugated Heteroacenes. *Chem.* **2018**, *4*, 2538−2570.
(9) Qiu, N.; Zhang, H.; Wan, X.; Li, C.; Ke, X.; Feng, H.; Kan, B.; Zhang, H.; Zhang, Q.; Lu, Y.; Chen, Y. A New Nonfullerene Electron Acceptor with a Ladder Type Backbone for High-Performance Organic Solar Cells. *Adv. Mater.* **2017**, *29*, 1604964.
(10) Hou, J.; Inganäs, O.; Friend, R. H.; Gao, F. Organic solar cells based on non-fullerene acceptors. *Nat. Mater.* **2018**, *17*, 119.
(11) Zhu, C.; Fang, L. Locking the Coplanar Conformation of π-Conjugated Molecules and Macromolecules Using Dynamic Noncovalent Bonds. *Macromol. Rapid Commun.* **2018**, *39*, 1700241.
(12) Scherf, U.; Müllen, K. Polyarylenes and poly (arylenevinylenes), 7. A soluble ladder polymer via bridging of functionalized poly (p-phenylene)-precursors. *Makromol. Chem., Rapid Commun.* **1991**, *12*, 489−497.
(13) Zou, Y.; Ji, X.; Cai, J.; Yuan, T.; Stanton, D. J.; Lin, Y.-H.; Naraghi, M.; Fang, L. Synthesis and Solution Processing of a Hydrogen-Bonded Ladder Polymer. *Chem.* **2017**, *2*, 139−152.
(14) Mirmohseni, A.; Oladegaragoze, A. Anti-corrosive properties of polyaniline coating on iron. *Synth. Met.* **2000**, *114*, 105−108.
(15) Gupta, V.; Miura, N. High performance electrochemical supercapacitor from electrochemically synthesized nanostructured polyaniline. *Mater. Lett.* **2006**, *60*, 1466−1469.
(16) MacDiarmid, A.; Yang, L.; Huang, W.; Humphrey, B. Polyaniline: Electrochemistry and application to rechargeable batteries. *Synth. Met.* **1987**, *18*, 393−398.
(17) Jiménez, P.; Levillain, E.; Alévêque, O.; Guyomard, D.; Lestriez, B.; Gaubicher, J. Lithium n-Doped Polyaniline as a High-Performance Electroactive Material for Rechargeable Batteries. *Angew. Chem., Int. Ed.* **2017**, *56*, 1553−1556.
(18) Zhao, L.; Zhao, L.; Xu, Y.; Qiu, T.; Zhi, L.; Shi, G. Polyaniline electrochromic devices with transparent graphene electrodes. *Electrochim. Acta* **2009**, *55*, 491−497.
(19) Akhtar, M.; Weakliem, H.; Paiste, R.; Gaughan, K. Polyaniline thin film electrochromic devices. *Synth. Met.* **1988**, *26*, 203−208.
(20) MacDiarmid, A. G. Synthetic metals": A novel role for organic polymers (Nobel lecture). *Angew. Chem., Int. Ed.* **2001**, *40*, 2581−2590.
(21) Javadi, H. H. S.; Treat, S. P.; Ginder, J. M.; Wolf, J. F.; Epstein, A. J. Aniline tetramers: Comparison with aniline octamer and polyaniline. *J. Phys. Chem. Solids* **1990**, *51*, 107−112.
(22) Wei, Z.; Faul, C. F. Aniline oligomers−architecture, function and new opportunities for nanostructured materials. *Macromol. Rapid Commun.* **2008**, *29*, 280−292.
(23) Ćirić-Marjanović, G. Recent advances in polyaniline research: Polymerization mechanisms, structural aspects, properties and applications. *Synth. Met.* **2013**, *177*, 1−47.
(24) Genies, E.; Boyle, A.; Lapkowski, M.; Tsintavis, C. Polyaniline: A historical survey. *Synth. Met.* **1990**, *36*, 139−182.
(25) MacDiarmid, A. G.; Zhou, Y.; Feng, J. Oligomers and isomers: new horizons in poly-anilines. *Synth. Met.* **1999**, *100*, 131−140.
(26) Lin, C.-W.; Li, R. L.; Robbennolt, S.; Yeung, M. T.; Akopov, G.; Kaner, R. B. Furthering Our Understanding of the Doping Mechanism in Conjugated Polymers Using Tetraaniline. *Macromolecules* **2017**, *50*, 5892−5897.
(27) Krinichnyi, V.; Konkin, A.; Monkman, A. Electron paramagnetic resonance study of spin centers related to charge transport in metallic polyaniline. *Synth. Met.* **2012**, *162*, 1147−1155.
(28) Cao, Y. Spectroscopic studies of acceptor and donor doping of polyaniline in the emeraldine base and pernigraniline forms. *Synth. Met.* **1990**, *35*, 319−332.
(29) Cao, Y.; Smith, P.; Heeger, A. Spectroscopic studies of polyaniline in solution and in spin-cast films. *Synth. Met.* **1989**, *32*, 263−281.
(30) D'Aprano, G.; Leclerc, M.; Zotti, G. Stabilization and characterization of pernigraniline salt: the" acid-doped" form of fully oxidized polyanilines. *Macromolecules* **1992**, *25*, 2145−2150.
(31) Bazito, F. F.; Silveira, L. T.; Torresi, R. M.; de Torresi, S. I. C. On the stabilization of conducting pernigraniline salt by the synthesis and oxidation of polyaniline in hydrophobic ionic liquids. *Phys. Chem. Chem. Phys.* **2008**, *10*, 1457−1462.
(32) MacDiarmid, A. G.; Manohar, S. K.; Masters, J. G.; Sun, Y.; Weiss, H.; Epstein, A. J. Polyaniline: Synthesis and properties of pernigraniline base. *Synth. Met.* **1991**, *41*, 621−626.
(33) Chandrakanthi, N.; Careem, M. Preparation and characterization of fully oxidized form of polyaniline. *Polym. Bull.* **2000**, *45*, 113−120.
(34) Chen, L.; Yu, Y.; Mao, H.; Lu, X.; Zhang, W.; Wei, Y. Synthesis of phenyl-capped aniline heptamer and its UV−vis spectral study. *Synth. Met.* **2005**, *149*, 129−134.
(35) Bogomolova, O. E.; Sergeyev, V. G. Acid Doping of Phenyl-Capped Aniline Dimer: Intermolecular Polaron Formation Mechanism and Its Applicability to Polyaniline. *J. Phys. Chem. A* **2018**, *122*, 461−469.
(36) Cao, Y.; Heeger, A. Charged solitons in pernigraniline. *Synth. Met.* **1990**, *39*, 205−214.
(37) Mažeikien, R.; Malinauskas, A. Electrochemical stability of polyaniline. *Eur. Polym. J.* **2002**, *38*, 1947−1952.
(38) Simoes, F.; Pocrifka, L.; Marchesi, L.; Pereira, E. Investigation of electrochemical degradation process in polyaniline/polystyrene sulfonated self-assembly films by impedance spectroscopy. *J. Phys. Chem. B* **2011**, *115*, 11092−11097.
(39) Stejskal, J.; Bober, P.; Trchová, M.; Horský, J.; Pilař, J.; Walterová, Z. The oxidation of aniline with p-benzoquinone and its impact on the preparation of the conducting polymer, polyaniline. *Synth. Met.* **2014**, *192*, 66−73.
(40) Jeon, J.-W.; Ma, Y.; Mike, J. F.; Shao, L.; Balbuena, P. B.; Lutkenhaus, J. L. Oxidatively stable polyaniline: polyacid electrodes for electrochemical energy storage. *Phys. Chem. Chem. Phys.* **2013**, *15*, 9654−9662.
(41) Jeon, J.-W.; O'Neal, J.; Shao, L.; Lutkenhaus, J. L. Charge storage in polymer acid-doped polyaniline-based layer-by-layer electrodes. *ACS Appl. Mater. Interfaces* **2013**, *5*, 10127−10136.

DOI: 10.1021/jacs.9b12626
J. Am. Chem. Soc. 2020, 142, 641−648

(42) Sandberg, M.; Hjertberg, T. E/Z isomerism in polyaniline, a model study. *Synth. Met.* **1989**, *29*, 257−264.
(43) Kalin, A. J.; Lee, J.; Fang, L. Annulation Reactions for Conjugated Ladder-Type Oligomers. *Synlett* **2018**, *29*, 993−998.
(44) Wakim, S.; Bouchard, J.; Blouin, N.; Michaud, A.; Leclerc, M. Synthesis of diindolocarbazoles by Ullmann reaction: a rapid route to ladder oligo (p-aniline) s. *Org. Lett.* **2004**, *6*, 3413−3416.
(45) Zheng, T.; Cai, Z.; Ho-Wu, R.; Yau, S. H.; Shaparov, V.; Goodson, T., III; Yu, L. Synthesis of Ladder-Type Thienoacenes and Their Electronic and Optical Properties. *J. Am. Chem. Soc.* **2016**, *138*, 868−875.
(46) Lee, J.; Li, H.; Kalin, A. J.; Yuan, T.; Wang, C.; Olson, T.; Li, H.; Fang, L. Extended Ladder-Type Benzo [k] tetraphene-Derived Oligomers. *Angew. Chem., Int. Ed.* **2017**, *56*, 13727−13731.
(47) Wang, Y.; Guo, H.; Ling, S.; Arrechea-Marcos, I.; Wang, Y.; López Navarrete, J. T.; Ortiz, R. P.; Guo, X. Ladder-type Heteroarenes: Up to 15 Rings with Five Imide Groups. *Angew. Chem.* **2017**, *129*, 10056−10061.
(48) Wang, Z.; Gu, P.; Liu, G.; Yao, H.; Wu, Y.; Li, Y.; Rakesh, G.; Zhu, J.; Fu, H.; Zhang, Q. A large pyrene-fused N-heteroacene: fifteen aromatic six-membered rings annulated in one row. *Chem. Commun.* **2017**, *53*, 7772−7775.
(49) Zeng, W.; Phan, H.; Herng, T. S.; Gopalakrishna, T. Y.; Aratani, N.; Zeng, Z.; Yamada, H.; Ding, J.; Wu, J. Rylene ribbons with unusual diradical character. *Chem.* **2017**, *2*, 81−92.
(50) Zou, Y.; Yuan, T.; Yao, H.; Frazier, D. J.; Stanton, D. J.; Sue, H.-J.; Fang, L. Solution-processable core-extended quinacridone derivatives with intact hydrogen bonds. *Org. Lett.* **2015**, *17*, 3146−3149.
(51) Zhang, X.-X.; Sadighi, J. P.; Mackewitz, T. W.; Buchwald, S. L. Efficient synthesis of well-defined, high molecular weight, and processible polyanilines under mild conditions via palladium-catalyzed amination. *J. Am. Chem. Soc.* **2000**, *122*, 7606−7607.
(52) Pullen, A. E.; Swager, T. M. Regiospecific copolyanilines from substituted oligoanilines: Electrochemical comparisons with random copolyanilines. *Macromolecules* **2001**, *34*, 812−816.
(53) Mills, B. M.; Fey, N.; Marszalek, T.; Pisula, W.; Rannou, P.; Faul, C. F. Exploring Redox States, Doping and Ordering of Electroactive Star-Shaped Oligo (aniline) s. *Chem. - Eur. J.* **2016**, *22*, 16950−16956.
(54) Sariciftci, N.; Kolbert, A.; Cao, Y.; Heeger, A.; Pines, A. Magnetic resonance evidence for metallic state in highly conducting polyaniline. *Synth. Met.* **1995**, *69*, 243−244.
(55) Huber, R. C.; Ferreira, A. S.; Thompson, R.; Kilbride, D.; Knutson, N. S.; Devi, L. S.; Toso, D. B.; Challa, J. R.; Zhou, Z. H.; Rubin, Y. Long-lived photoinduced polaron formation in conjugated polyelectrolyte-fullerene assemblies. *Science* **2015**, *348*, 1340−1343.
(56) Beldjoudi, Y.; Osorio-Román, I.; Nascimento, M. A.; Rawson, J. M. A fluorescent dithiadiazolyl radical: structure and optical properties of phenanthrenyl dithiadiazolyl in solution and polymer composites. *J. Mater. Chem. C* **2017**, *5*, 2794−2799.
(57) Rajca, A. Organic Diradicals and Polyradicals - from Spin Coupling to Magnetism. *Chem. Rev.* **1994**, *94*, 871−893.
(58) Earney, J.; Finn, C.; Najafabadi, B. Van Vleck temperature independent paramagnetism in some rare earth double nitrates. *J. Phys. C: Solid State Phys.* **1971**, *4*, 1013.
(59) Carrington, A. The temperature-independent paramagnetism of permanganate and related complexes. *Mol. Phys.* **1960**, *3*, 271−275.
(60) Goldberg, I.; Crowe, H.; Newman, P.; Heeger, A.; MacDiarmid, A. Electron spin resonance of polyacetylene and AsF5-doped polyacetylene. *J. Chem. Phys.* **1979**, *70*, 1132−1136.
(61) Kang, K.; Watanabe, S.; Broch, K.; Sepe, A.; Brown, A.; Nasrallah, I.; Nikolka, M.; Fei, Z.; Heeney, M.; Matsumoto, D. 2D coherent charge transport in highly ordered conducting polymers doped by solid state diffusion. *Nat. Mater.* **2016**, *15*, 896−902.
(62) Tanaka, H.; Hirate, M.; Watanabe, S.; Kuroda, S. i. Microscopic signature of metallic state in semicrystalline conjugated polymers doped with fluoroalkylsilane molecules. *Adv. Mater.* **2014**, *26*, 2376−2383.
(63) Zheng, Y.; Miao, M. s.; Dantelle, G.; Eisenmenger, N. D.; Wu, G.; Yavuz, I.; Chabinyc, M. L.; Houk, K. N.; Wudl, F. A Solid-State Effect Responsible for an Organic Quintet State at Room Temperature and Ambient Pressure. *Adv. Mater.* **2015**, *27*, 1718−1723.
(64) Angelopoulos, M.; Dipietro, R.; Zheng, W.; MacDiarmid, A.; Epstem, A. Effect of selected processing parameters on solution properties and morphology of polyaniline and impact on conductivity. *Synth. Met.* **1997**, *84*, 35−39.
(65) Zeng, Z.; Shi, X.; Chi, C.; Lopez Navarrete, J. T.; Casado, J.; Wu, J. Pro-aromatic and anti-aromatic pi-conjugated molecules: an irresistible wish to be diradicals. *Chem. Soc. Rev.* **2015**, *44*, 6578−96.
(66) Chow, C. H. E.; Han, Y.; Phan, H.; Wu, J. Nitrogen-doped heptazethrene and octazethrene diradicaloids. *Chem. Commun.* **2019**, *55*, 9100−9103.
(67) Wang, L.; Zhang, L.; Fang, Y.; Zhao, Y.; Tan, G.; Wang, X. Orthogonal Oriented Bisanthrancene-Bridged Bis (Triarylamine) Diradical Dications: Isolation, Characterizations and Crystal Structures. *Chem. - Asian J.* **2019**, *14*, 1708−1711.
(68) Hu, X.; Chen, H.; Zhao, L.; Miao, M.; Han, J.; Wang, J.; Guo, J.; Hu, Y.; Zheng, Y. Nitrogen analogues of Chichibabin's and Müller's hydrocarbons with small singlet−triplet energy gaps. *Chem. Commun.* **2019**, *55*, 7812−7815.
(69) Rudebusch, G. E.; Zafra, J. L.; Jorner, K.; Fukuda, K.; Marshall, J. L.; Arrechea-Marcos, I.; Espejo, G. L.; Ortiz, R. P.; Gómez-García, C. J.; Zakharov, L. N. Diindeno-fusion of an anthracene as a design strategy for stable organic biradicals. *Nat. Chem.* **2016**, *8*, 753.
(70) Dressler, J. J.; Teraoka, M.; Espejo, G. L.; Kishi, R.; Takamuku, S.; Gómez-García, C. J.; Zakharov, L. N.; Nakano, M.; Casado, J.; Haley, M. M. Thiophene and its sulfur inhibit indenoindenodibenzothiophene diradicals from low-energy lying thermal triplets. *Nat. Chem.* **2018**, *10*, 1134.
(71) Guo, Z.-H.; Ai, N.; McBroom, C. R.; Yuan, T.; Lin, Y.-H.; Roders, M.; Zhu, C.; Ayzner, A. L.; Pei, J.; Fang, L. A side-chain engineering approach to solvent-resistant semiconducting polymer thin films. *Polym. Chem.* **2016**, *7*, 648−655.

DOI: 10.1021/jacs.9b12626
J. Am. Chem. Soc. 2020, 142, 641−648